Of spin and charge in the cuprates

Grüninger, Markus Uwe; Sawatzky, G.A

Link to publication in University of Groningen/UMCG research database

Chapter 7

Magneto-Elastic Polarons in Low Doped YBa$_2$Cu$_3$O$_{6+\delta}$

After having analyzed the optical conductivity spectrum of undoped YBa$_2$Cu$_3$O$_6$ in the preceding chapters, we now turn to the study of low doped YBa$_2$Cu$_3$O$_x$ (6.0 ≤ x ≤ 6.2) in the far- and mid-infrared frequency range. We observe that very light chemical doping with oxygen introduces localized charge carriers in the form of magneto-elastic polarons, i.e., holes which are strongly coupled both to the vibrational and magnetic degrees of freedom.

7.1   Introduction

The important question, whether the Hubbard model or its low energy version, the *t-J* model, capture the physics relevant to obtain a high T$_c$ superconductor is still open. The low energy dynamics and in particular the optical conductivity $\sigma(\omega)$ of holes doped into a 2D $S = 1/2$ square-lattice antiferromagnet have been the subject of intensive theoretical investigations [60–62, 242, 243, 502]. We reproduce an exact diagonalization result for $\sigma(\omega)$ from Eder, Wróbel and Ohta [242] in Fig. 7.1. Strong interactions with the antiferromagnetic background renormalize the bandwidth drastically. The Drude weight is suppressed and a large part of the spectral weight is transferred to incoherent excitations, smeared out over a wide frequency range (up to about $6t$ in Fig. 7.1). Good agreement has been obtained between these exact diagonalization studies of the *t-J* model [242] and analytical calculations for spin-bag quasiparticles [243]. There, the very broad incoherent contribution is identified with internal excitations of spin-bags or spin polarons. The hole moves *incoherently* on an energy scale $\sim t$ within a region of reduced staggered magnetization (see Fig. 2.19 on page 51). The hole plus the defect region move *coherently* on the lower energy scale $\sim J$, which is possible due to quantum spin fluctuations. In 1D, a robust Drude peak is obtained in exact diagonalization studies [503], but only a negligible amount of spectral weight is found at finite frequencies [503], contrary to the 2D case. The quasiparticles decay into spinons and holons in 1D and hence there is no "dressing" of the holons with
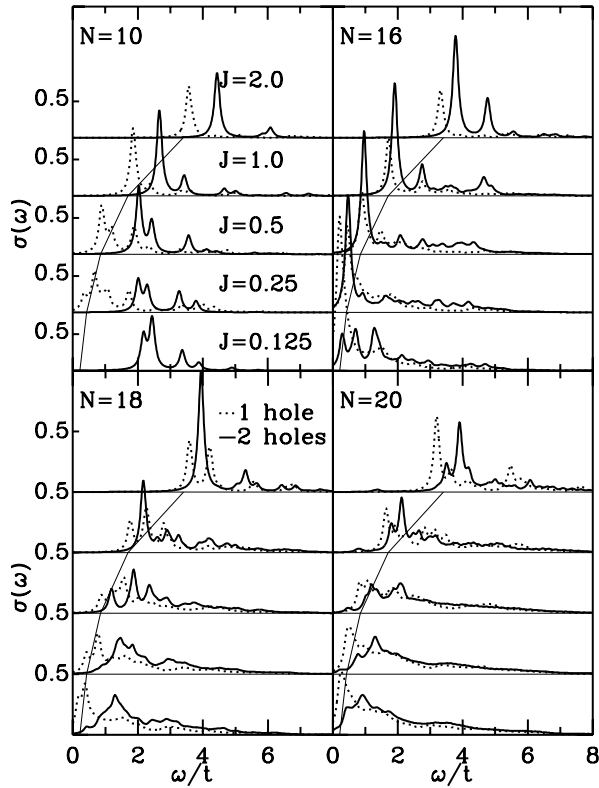
Figure 7.1: *Exact diagonalization result of the optical conductivity spectrum of one or two holes doped into a cluster of size N for the $t-J$ model, reproduced from Eder, Wróbel and Ohta [242]. The relevant parameter set for the cuprates is $J=0.25t$. The thin solid line denotes $\omega=1.7J$.*
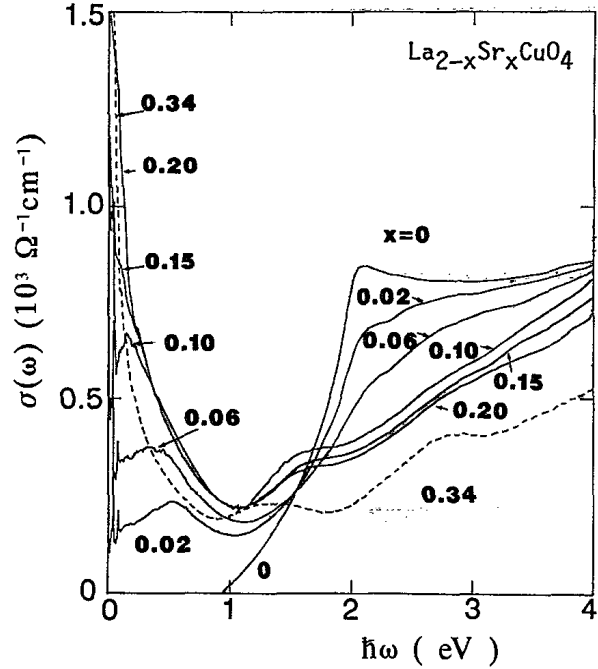
Figure 7.2: *Doping dependence of $\sigma(\omega)$ of $La_{2-x}Sr_xCuO_4$ at 300 K, reproduced from Uchida et al. [65].*

spin excitations, which supports the view that the incoherent excitations of the dressing are strongly related to the mid-infrared absorption in 2D [60]. However, one has to keep in mind that a photon creates an electron-hole excitation, *i.e.*, it does not couple directly to holons, and that the energy and the momentum of the electron-hole pair can be distributed among holons and spinons.

Experimentally, $\sigma(\omega)$ deviates from the free electron Drude form at *all* doping levels in *all* 2D cuprates [25,44,65]. Spectra of $\sigma(\omega)$ over a wide doping range are summarized in Figs. 7.2 and 7.3 for $La_{2-x}Sr_xCuO_4$ [65] and $YBa_2Cu_3O_{6+y}$ [29]. Note that the sample temperature is 300 K in both figures. In the metallic regime, the non-Drude behavior has been approached in a microscopically meaningful way by extracting the frequency dependent self-energy (usually in the form of scattering rate and effective mass) from the experimental spectra. It has been claimed [60–62] that the t-J model describes $\sigma(\omega)$ in the metallic regime well. The experimental data of the low doped insulating state were
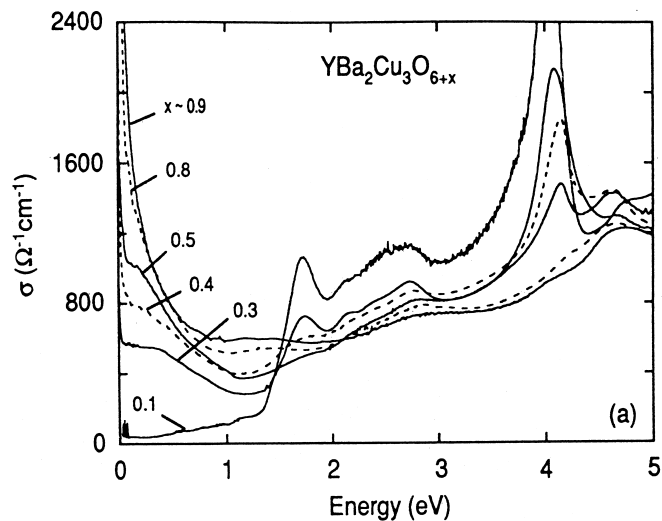
Figure 7.3: *Doping dependence of $\sigma(\omega)$ of $YBa_2Cu_3O_{6+y}$ at 300 K, reproduced from Cooper et al. [29].*
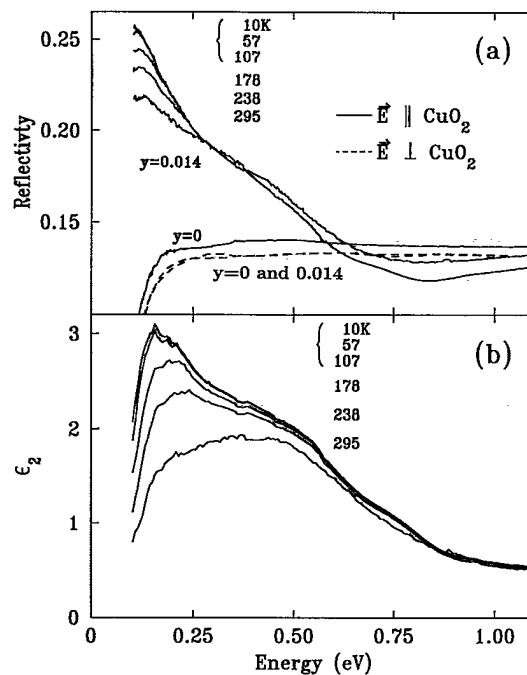
Figure 7.4: *Top: reflectivity spectra of undoped $(y=0)$ and low doped $(y=0.014)$ La_2CuO_{4+y}. Bottom: temperature dependence of $\epsilon''(\omega)$ for $E \parallel CuO_2$ and $y=0.014$. Reproduced from Falck et al. [45].*
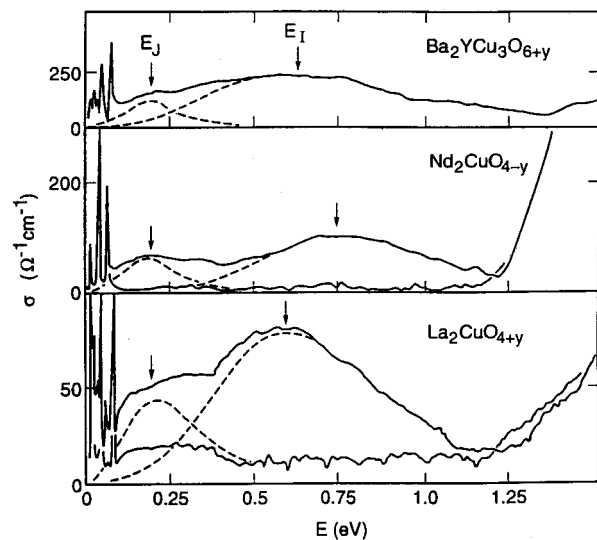
Figure 7.5: *Spectra of $\sigma(\omega)$ of different low doped cuprates, reproduced from Thomas et al. [504]. Note that the sample temperatures are 300 K for $YBa_2Cu_3O_{6+y}$ and 4 K for the others.*
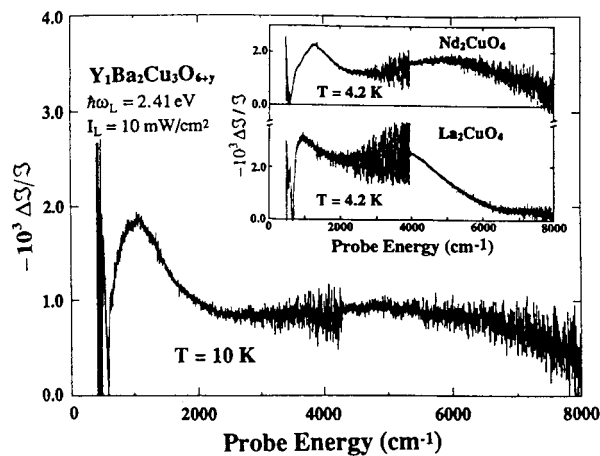
Figure 7.6: *Low temperature photo-induced absorption spectra of powder samples, reproduced from Li, Kim and Cheong [506].*

discussed in more conventional terms, neglecting the electronic correlations. Two distinct peaks at about 1200 and 5000 – 6000 cm^{-1} have been found in various low doped cuprates in both reflectance spectra of chemically doped single crystals [45, 504] (see Figs. 7.4 and 7.5) and photo-induced absorption data (photo doping) [505, 506]. Different studies of photo-induced absorption disagree on the spectral weight of the two peaks, showing, *e.g.*, predominantly the lower (upper) peak in YBa$_2$Cu$_3$O$_{6+y}$ (La$_{2-x}$Sr$_x$CuO$_4$) [507], which has led to some confusion concerning the assignment [507]. Recently, the simultaneous presence of both peaks in photo-induced absorption data has been demonstrated by Li, Kim and Cheong [506] in various cuprates (see Fig. 7.6).

For both doping induced peaks interpretations in terms of impurities and lattice degrees of freedom were proposed. Falck and co-workers [45] (see Fig. 7.4) interpreted the lower peak in La$_2$CuO$_{4.014}$ as a photo-ionization process of holes bound to oxygen impurities forming polaronic impurities, *i.e.*, involving a lattice relaxation. Thomas and collaborators [504] (see Fig. 7.5) attributed the *higher* peak at about 5000 – 6000 cm^{-1} to an impurity ionization process, and suggested a magnetic excitation of a carrier bound to an impurity as origin for the 1200 cm^{-1} peak because its frequency is close to the exchange constant J. However, the theoretical oscillator strength of this excitation is too small compared to experiment [509]. These assignments seem to indicate that at low doping levels the hole dynamics are dominated by impurities and a coupling to the lattice, with the amusing consequence that the theoretically widely studied case of a "*single* hole in an antiferromagnet" only seems to apply to experimental data at higher doping levels [60–62].

So far, there have been no detailed experimental studies of $\sigma(\omega)$ in the very low doping regime. We present low temperature spectra of eight different samples of YBa$_2$Cu$_3$O$_x$ with $x < 6.1$, corresponding to an effective carrier density $\leq 5 \cdot 10^{19}$ cm^{-3}. This allows us to draw the doping dependence of $\sigma(\omega)$ on a logarithmic scale in Fig. 7.7. Data for $x \geq 6.1$ have been reproduced from Münzel [501]. The $x = 6.3$ data agree favorably with the results of Thomas and co-workers [504] (see Fig. 7.5; note the different temperatures). Here, we concentrate on the low doping regime which is indicated by the grey area. Compared to the undoped case, the low doping level of our samples hardly affects the far-infrared spectrum, where a Drude contribution can only be inferred indirectly (see below). Yet, we observe drastic changes in the mid-infrared frequency range (see Fig. 7.8). A broad background arises which is attributed to the incoherent internal excitations of spin polarons. A strongly temperature dependent peak at 1050 cm^{-1} is interpreted as a photo-ionization process of a localized *magneto-elastic* polaron, *i.e.*, not of a bare hole, but of a quasiparticle dressed by phonons *and* magnons. The evolution of these features with doping is studied for $x = 6.1$, 6.2 and 6.3.

Sample Preparation

Single crystals of YBa$_2$Cu$_3$O$_x$ were grown in Y$_2$O$_3$ stabilized ZrO$_2$ (YSZ) crucibles as described elsewhere [397]. In order to reduce the oxygen content the samples were annealed (i) in ultra high vacuum at 700°C (undoped case), (ii) between 2 and 5 days in a flow of high purity Argon (99.998 %) at 750°C ($x < 6.1$), or (iii) according to the calibration of
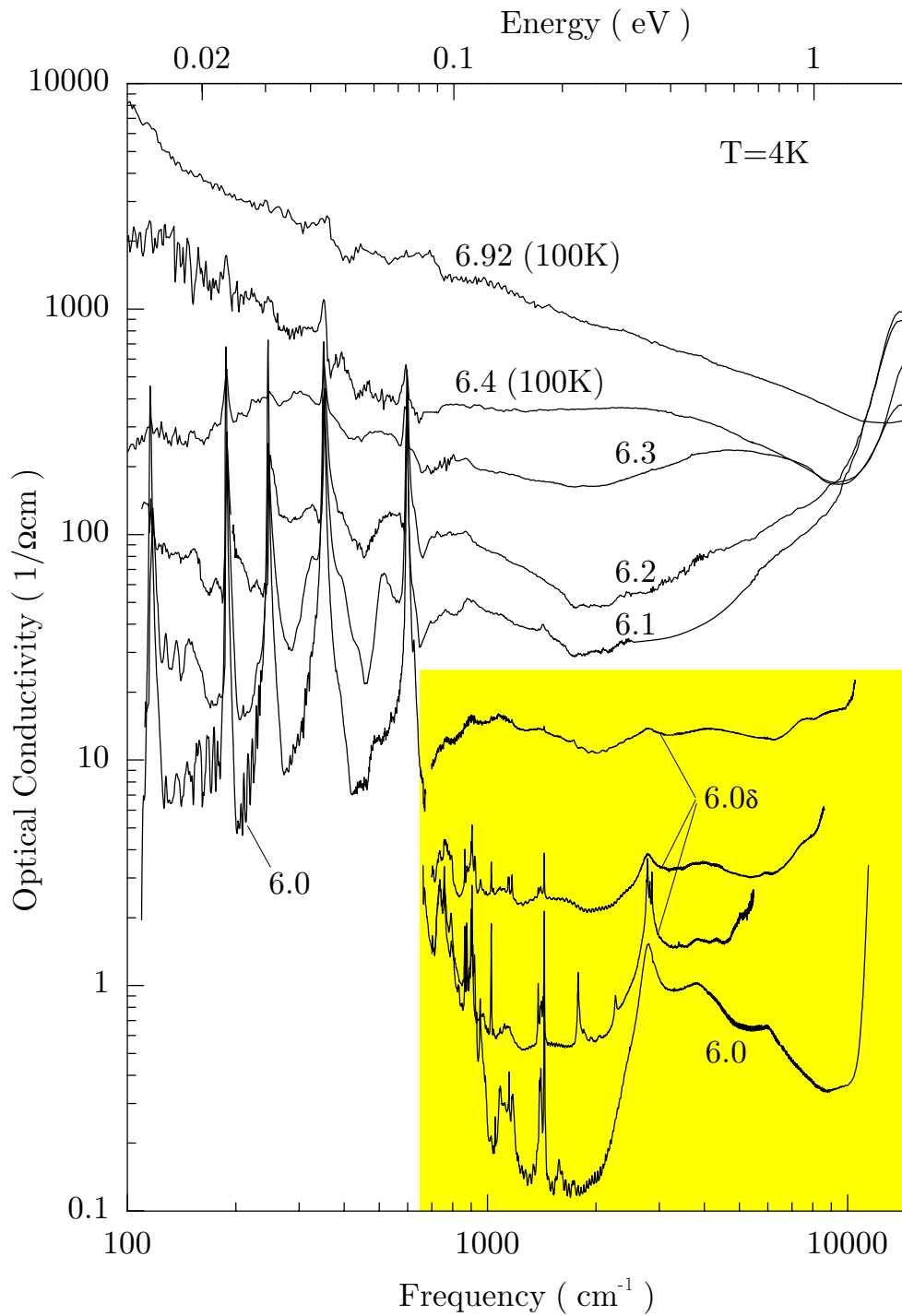
Figure 7.7: *Doping dependence of $\sigma(\omega)$ of $YBa_2Cu_3O_x$ at 4 K (100 K for the superconducting samples with $x = 6.4$ and 6.92). Data for $x \geq 6.1$ are reproduced from Münzel [501]. The $x = 6.3$ data agree favorably with the results of Thomas and co-workers [504] (see Fig. 7.5; note the different temperatures). Here, we focus on the low doping regime indicated by the grey area.*
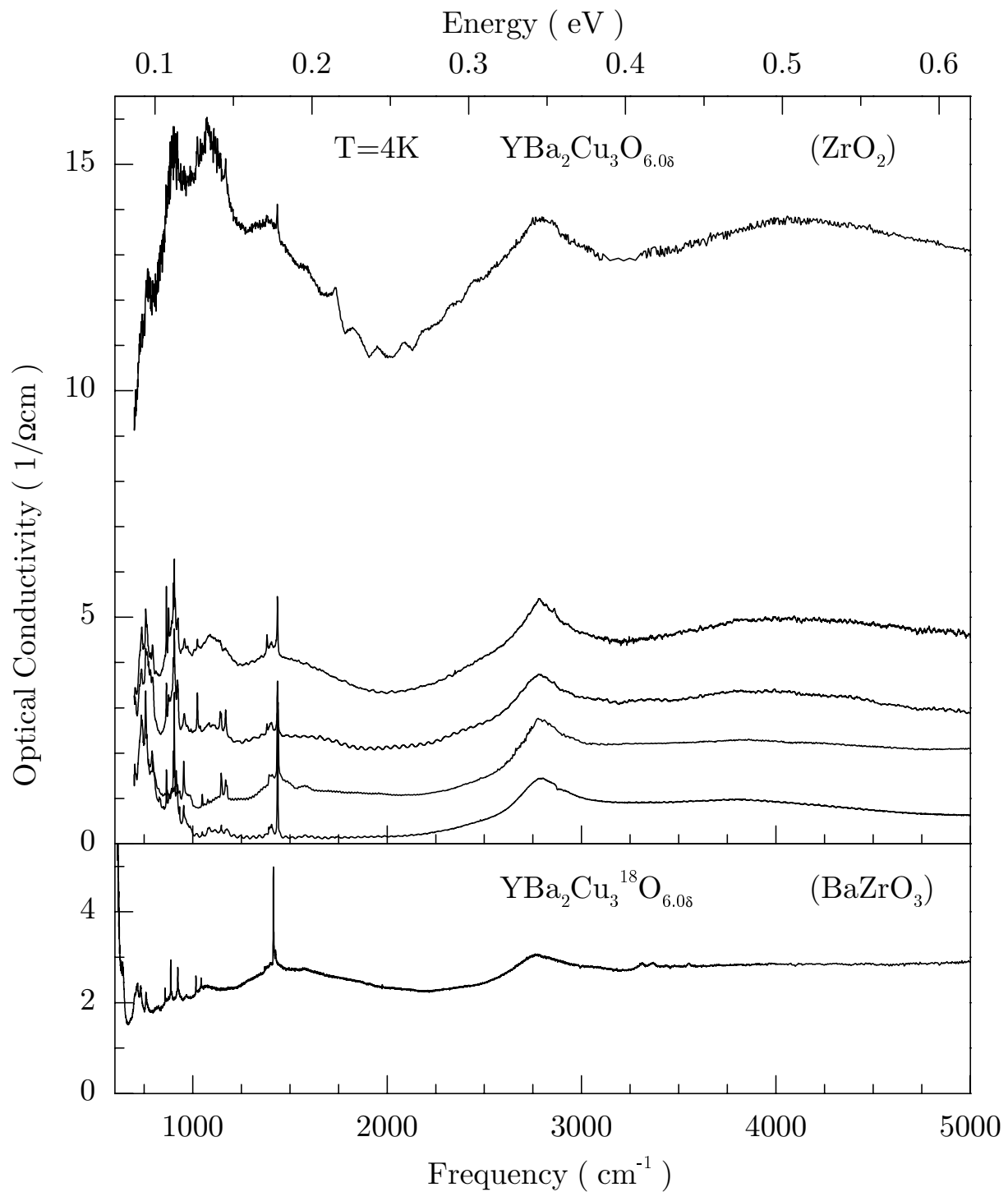
Figure 7.8: *Mid-infrared $\sigma(\omega)$ spectra of $YBa_2Cu_3O_x$ in the low doping regime $x < 6.1$ at 4 K. Note the very low values of $\sigma(\omega)$. Top panel: samples grown in ZrO_2 crucibles; bottom panel: oxygen isotope substituted sample of $YBa_2Cu_3{}^{18}O_6$ grown in a $BaZrO_3$ crucible.*

Figure 7.9: *Doping induced changes in $\sigma(\omega)$ of YBa$_2$Cu$_3$O$_x$ with $x < 6.1$ at 4 K. These curves have been obtained by subtracting the lowest spectrum in the top panel of Fig. 7.8 from all the others. The arrows indicate that it is not obvious whether the spectra show one o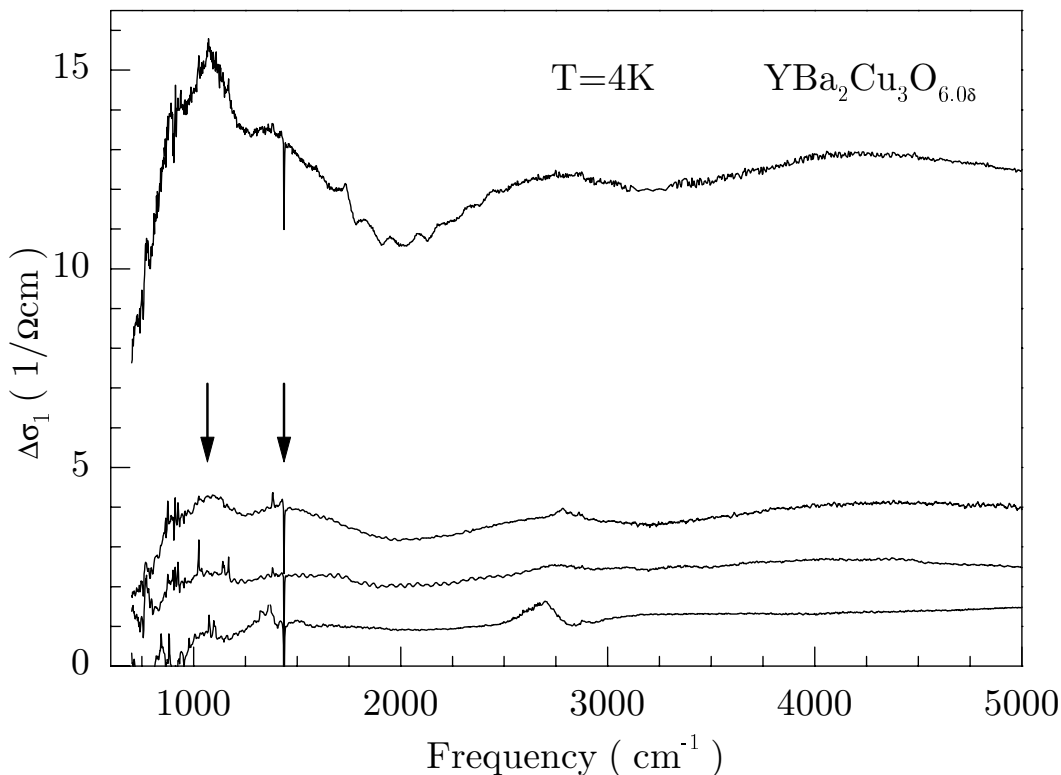r two doping induced peaks between 1000 and 1500 cm^{-1}. Part of the structure at 1000 cm^{-1} can be due to differences in spectral weight of multi-phonon absorption.*

Lindemer and co-workers [396] ($6.1 \leq x \leq 6.3$). The full exchange of the oxygen isotope in a sample grown in a BaZrO$_3$ (BZO) crucible [117] was described on page 106. Reflection and transmission measurements were carried out between 30 cm^{-1} and 12000 cm^{-1} for temperatures ranging from 4 to 300 K. We calculated $\sigma(\omega)$ either by (a) inverting the Fresnel equations for the experimentally measured transmission and reflection data, or (b) in the case of strong absorption ($\sigma(\omega) \geq 20\,\Omega^{-1}\text{cm}^{-1}$) by using a Kramers-Kronig analysis of reflectivity data measured up to 6 eV [433]. The small remnants of interference fringes in some of the calculated spectra of $\sigma(\omega)$ are artefacts caused by deviations of the measured data from the in (a) assumed ideal case of absolutely flat and plane parallel surfaces.

7.2 Discussion

In the absence of doping $\sigma(\omega)$ of YBa$_2$Cu$_3$O$_{6.0}$ shows phonons below 650 cm^{-1} and the charge transfer gap at about 12000 cm^{-1} (see preceding chapters). The electronic low energy excitations are magnetic for zero doping, and they produce spectral weight in the gap
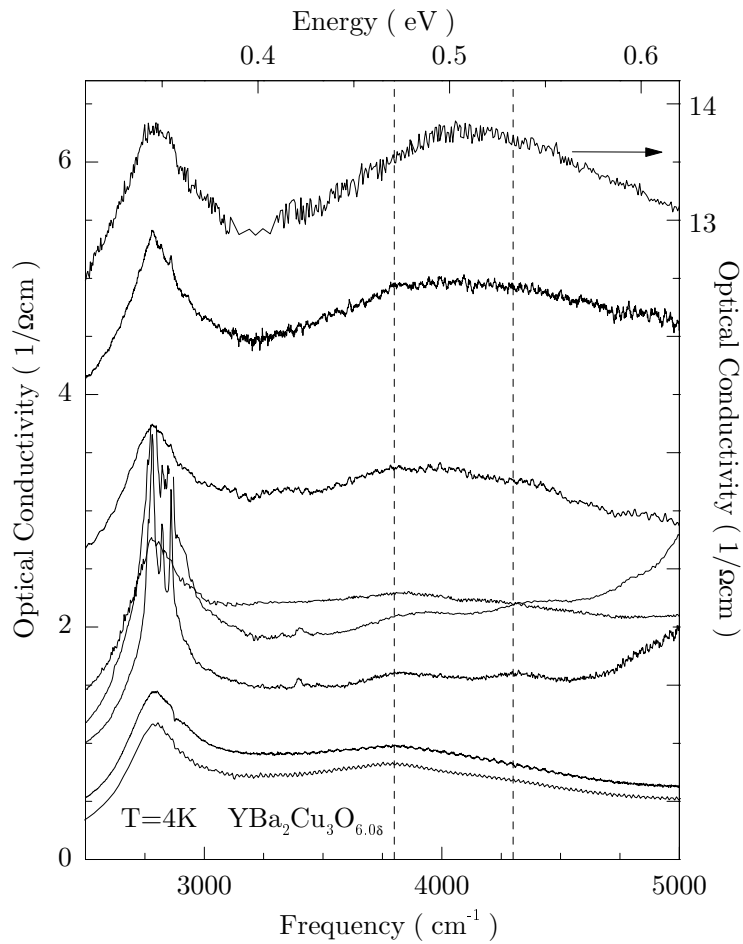
Figure 7.10: *At about 4000 cm^{-1} a strong doping induced increase of spectral weight is observed. Note that the top curve has been shifted down and refers to the right axis. The two peaks at 3825 and 4325 cm^{-1} (dashed lines) can only be distinguished at low doping concentrations.*

above 2000 cm^{-1} in the form of bimagnon-plus-phonon absorption [224, 225] (see chapter 5). Experimentally, the undoped case is realized in the sample annealed in ultra high vacuum (lowest curve in the top panel of Fig. 7.8). All other curves in Fig. 7.8 represent the influence of very low doping on $\sigma(\omega)$ (top/bottom panel: samples with O isotope ^{16}O/^{18}O). Note that all samples are still very close to the undoped limit YBa$_2$Cu$_3$O$_{6.0}$, as $\sigma(\omega)$ in YBa$_2$Cu$_3$O$_{6.1}$ already amounts to 25 – 100 Ω^{-1}cm^{-1} (see Fig. 7.7). In order to focus on the doping induced *changes*, we subtracted the $\sigma(\omega)$ spectrum of the undoped sample from the data of the others (see Fig. 7.9). Most prominent are: (a) a very broad, flat background, (b) a strong peak at about 1050 cm^{-1}, and (c) an increase in oscillator strength of bimagnon-plus-phonon absorption. These data agree with the above mentioned results of previous studies of higher doping levels, which concentrate on peaks at about 1300 ± 250 and 5000 ± 400 cm^{-1} (values for YBa$_2$Cu$_3$O$_{6+y}$) [45, 504] (see Figs. 7.4 and 7.5). At the same time, our spectra reveal a strong contribution of the broad background, which is observed for the first time.

Let us first address the magnetic excitations. In the cuprates, direct magnon absorption is not allowed for symmetry reasons. This selection rule can be relaxed by either exciting a phonon simultaneously [224, 225] or by adding impurities as, *e.g.*, Zn [429] (see Fig. 5.8 on
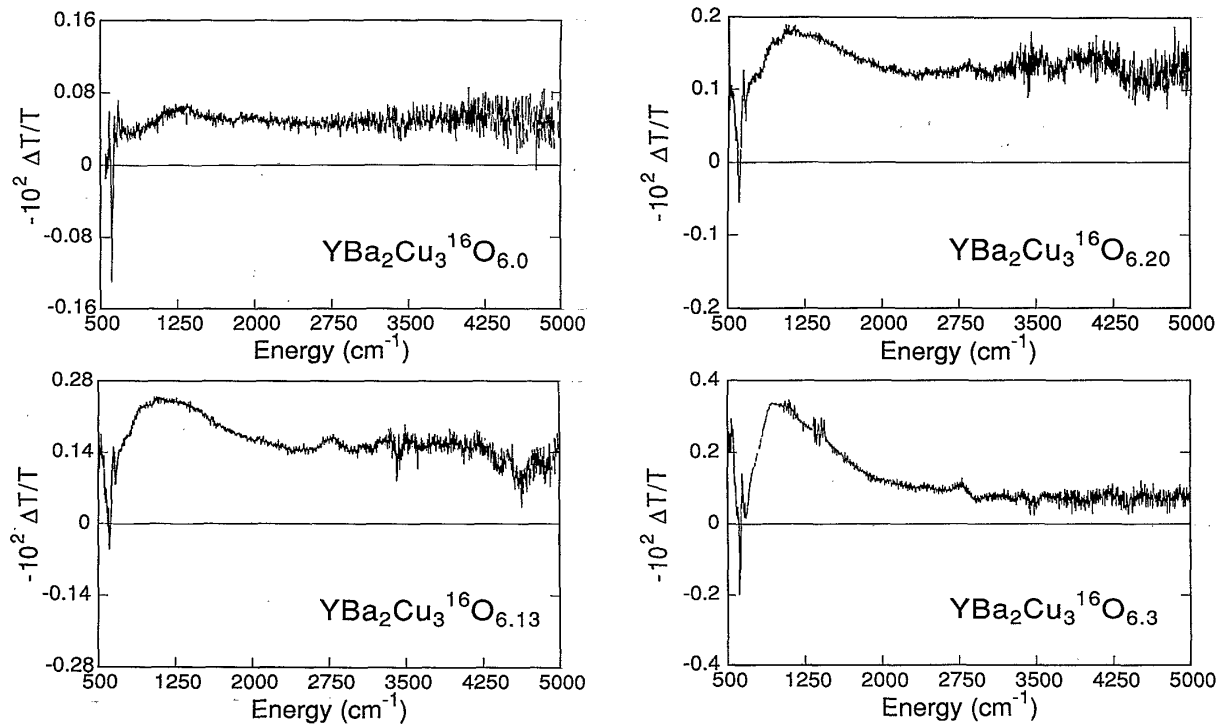
Figure 7.11: *Photo-induced absorption spectra of powder samples of $YBa_2Cu_3O_x$ mixed with CsI for temperatures in the range from 7 to 27 K, reproduced from Ye et al. [381]. Note the photo-induced bimagnon-plus-phonon absorption peak at 2800 cm^{-1} for x > 6. The data agree very well with our results for chemical doping, see Fig. 7.9.*

page 138). However, neither the O impurities located about 4 Å away from the spins of the CuO_2 layers nor the holes doped into these layers do the same: we do not find any indication for direct bimagnon absorption below the bimagnon-plus-phonon peak. Unexpectedly, the spectral weight of *bimagnon-plus-phonon* excitations increases with doping, which cannot be explained by symmetry breaking effects. In chapter 5 a strong increase of spectral weight of magnetic excitations with increasing temperature was observed and attributed to enhanced spin fluctuations. It is hence tempting to speculate about a similar origin here, namely an enhancement of spin fluctuations caused by the doped holes.

Bimagnon-plus-phonon absorption can also be detected in low doping data of other authors. We identify a so far not understood weak peak in low doped $Nd_2CuO_{4-\delta}$ at 2750 cm^{-1} [504] (see Fig. 7.5) with the bimagnon-plus-phonon peak observed at the same frequency by Perkins and co-workers [226] in Nd_2CuO_4. In Fig. 7.11 we reproduce photo-induced absorption spectra of $YBa_2Cu_3O_x$ from Ye and collaborators [381], which are in excellent agreement with our results. Note the different scales of the four panels. All spectra with x > 6 show an enhancement of bimagnon-plus-phonon absorption around 2800 cm^{-1}, which had not been realized thus far. The photo-induced absorption spectra further agree with our results by showing a peak *above* 1250 cm^{-1} at doping levels very

close to the insulating state (upper left panel of Fig. 7.11) and a peak around 1000 cm^{-1} for higher doping concentrations. A similar behavior is apparent in Fig. 7.8; note also the arrows in Fig. 7.9. Ye and collaborators [381] had attributed this absorption to excitations within the Cu-O chains. However, the observation of a peak at this frequency in *all* low doped cuprates (see Figs. 7.4 and 7.5) identifies it as an intrinsic feature of the carriers doped into the CuO$_2$ planes.

At higher frequencies, our results indicate an increase of spectral weight at about 4000 cm^{-1} which can be traced back to the features at 3825 and 4325 cm^{-1} in undoped samples (see Fig. 7.10). However, the above mentioned feature at 5000 $\pm$ 400 cm^{-1} [504] does not coincide with any magnetic peak in the undoped compounds. This is particularly clear in the case of Nd$_2$CuO$_{4-y}$, in which the bimagnon-plus-phonon peaks are observed at a lower frequency than in La$_2$CuO$_4$ [226,227], whereas the doping induced peak is much higher in frequency than in La$_{2-x}$Sr$_x$CuO$_4$ [504] (see Fig. 7.5).

The doping induced broad background reflects the strongly correlated nature of the doped carriers. In an ordinary semiconductor doping gives rise to an impurity band with a well defined peak frequency within the semiconducting gap. Our data show that already low doping produces spectral weight in the *whole* frequency range below the charge transfer gap in YBa$_2$Cu$_3$O$_{6.0\delta}$. This can only be explained by strong correlations. The *t-J* model for example shows incoherent excitations for frequencies up to $6t$ [242] (see Fig. 7.1).

The key to the interpretation of the 1050 cm^{-1} peak can be found in its temperature dependence (see Fig. 7.12; note the different absolute values of the three panels). The spectral weight of the 1050 cm^{-1} peak decreases strongly with increasing temperature, and at 300 K only the broad background is left. The spectral weight is transferred to $\omega=0$, which can only be shown indirectly. Due to the very low doping level, no Drude peak is observed in the measured frequency range down to 30 cm^{-1}. Absorption is low and the samples are transparent at all temperatures. This allows to observe and analyze interference fringes which occur due to multiple reflectance on the sample surfaces (see Fig. 7.13). The position of a given interference minimum is proportional to $1/nd$ (neglecting absorption), where n is the refractive index and d the sample thickness. Neglecting small changes in d with temperature, we can deduce the temperature dependence of n from the shift of an interference minimum (the arrows in Fig. 7.13 are guides to the eye). In the undoped case $x = 6.0$ (left panel) the minimum shifts to lower frequencies with increasing temperature, *i.e.*, *n increases*. For finite doping (mid panel, ^{18}O) n first increases from 4 to 100 K as in the undoped case, but for higher temperatures it starts to *decrease*. At a doping level corresponding to the highest curve in Fig. 7.8 *n decreases* with increasing temperature (right panel of Fig. 7.13). This claim can be substantiated by analyzing the full interference spectrum. As discussed in chapter 4 it is possible to determine the phonon-polariton dispersion from the interference spectrum. For the two samples of the left and mid panel of Fig. 7.13 the result is displayed in Fig. 7.14. The large period of the interferences in the higher doped sample (right panel of Fig. 7.13) prohibited such an analysis. We recall that the slope of the dispersion is given by $(\epsilon')^{-1/2}$. In the undoped sample, the 300 K dispersion curve is lying *below* the 4 K data, most likely due to the redshift of the phonon at 115 cm^{-1} with increasing temperature. The same is true for
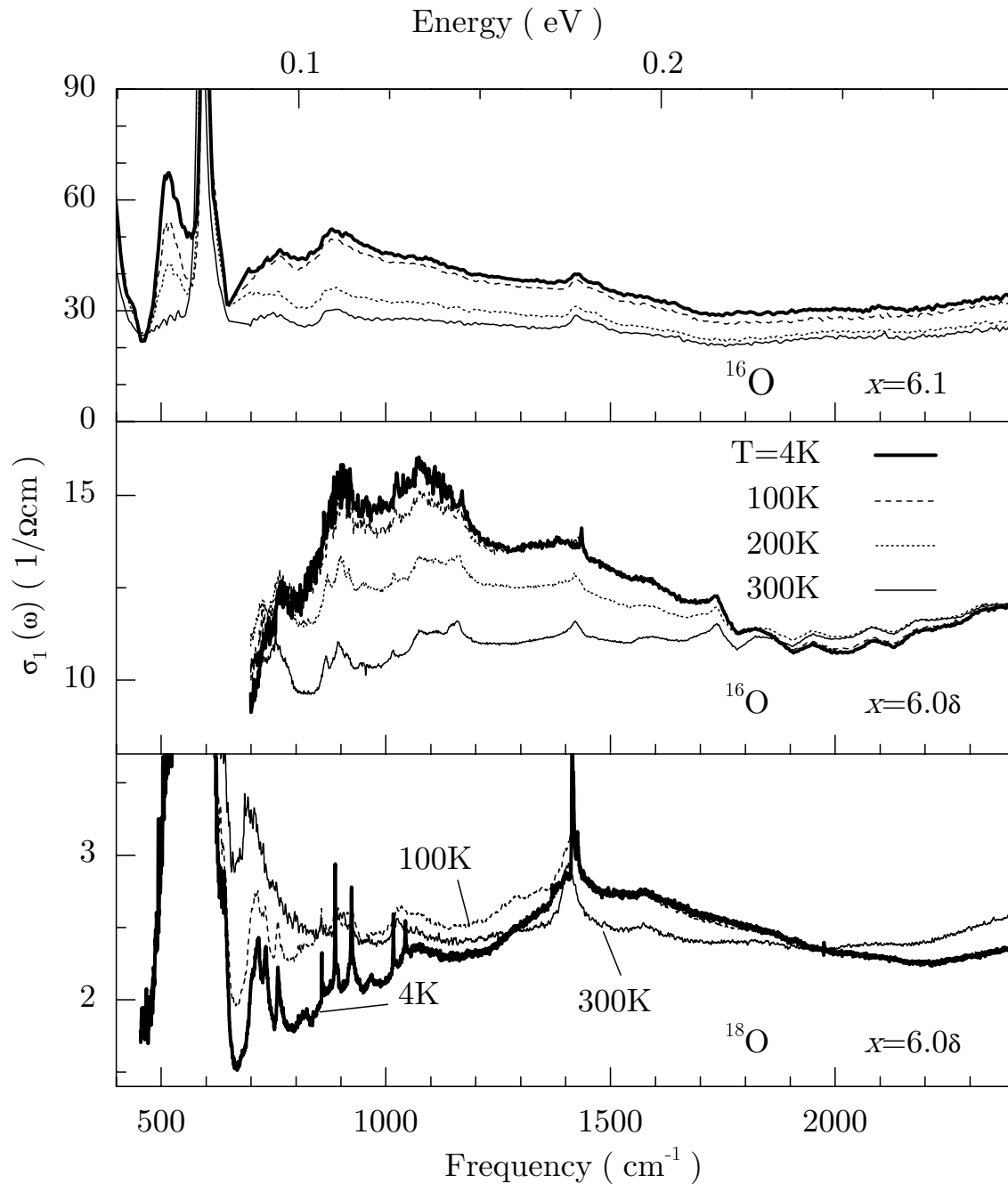
Figure 7.12: *Temperature dependence of* $\sigma(\omega)$ *of* $YBa_2Cu_3O_x$ *for different low doping concentrations. Note the different absolute values of* $\sigma(\omega)$ *in the three panels. Bottom panel: data of* $YBa_2Cu_3{}^{18}O_{6.0\delta}$*. Data in mid panel correspond to the highest curve in Fig. 7.8. The curve for* $x=6.1$ *(top panel) is reproduced from Münzel [501] and was obtained via a Kramers-Kronig analysis of reflectance data, whereas data in the lower panels were calculated from transmittance and reflectance measurements.*

the lightly doped sample between $\omega = 85 - 100\,\text{cm}^{-1}$, but at lower frequencies and wave vectors the opposite is the case, indicating a smaller value of ϵ'. This decrease of n or ϵ' with increasing temperature in the doped samples can be attributed to the negative contribution of the Drude peak to the real part of the dielectric constant. This is corroborated by the simulation plotted in the right panel of Fig. 7.14. Here, the solid line has been derived from a fit of the 4 K reflectivity data of an undoped sample. The dashed line is obtained by adding a small Drude term with $\omega_0 = 0$, $\omega_p = 100\,\text{cm}^{-1}$ and $\gamma = 25\,\text{cm}^{-1}$ to the fit, and by using the experimental 4 to 300 K redshift of $0.9\,\text{cm}^{-1}$ for the $115\,\text{cm}^{-1}$ phonon. The simulation agrees very well with the experimental data of the doped sample. Hence we conclude that spectral weight is transferred from the mid-infrared to $\omega=0$. In Ref. [45] the same conclusion was drawn from an analysis of the temperature dependence of the Hall coefficient.

The spectral weight transfer to $\omega = 0$ points towards a photo-ionization process of a polaronic impurity [45]. Let us describe this process in more detail. We start by recalling that the scale for the coherent motion of a spin polaron is set to J by the strong interactions of a doped hole with the antiferromagnetic spin background. As this motion is slow, already a moderate coupling λ to the lattice is sufficient to distort the lattice around the spin polaron, *i.e.*, to form a *magneto-elastic* polaron. The doped hole now has to drag along a cloud of both magnetic and vibrational excitations, which makes it so heavy that it can be trapped easily by impurities. The polaronic impurity hence denotes an impurity-bound state of a hole, around which both the lattice and the spin background have relaxed. The above mentioned optical photo-ionization peak observed at $1050\,\text{cm}^{-1}$ corresponds to a process, in which the bare hole is kicked off the impurity before the lattice can react. On contrary, thermal ionization is an adiabatic process, and therefore the thermal activation energy is much smaller: the presence of thermally activated phonons at elevated temperatures washes out the potential well of the lattice part of the polaron, and the peak vanishes already at 300 K. In photo-induced absorption measurements [505, 506, 508] the decrease of spectral weight with increasing temperature of the $1200\,\text{cm}^{-1}$ peak starts already at much lower temperatures, suggesting a smaller binding energy for photo-carriers [45] as compared to chemical doping. At first sight one might expect that the frequency of the photo-ionization process varies strongly among different cuprates due to, *e.g.*, the differences in distance of the impurity to the CuO$_2$ layers. However, the peak frequency is mainly determined by the relaxation of the lattice, especially of the O phonon modes of the CuO$_2$ layers, which are similar among different cuprates. In an LDA+U calculation on a 2×2 supercell of La$_{2-x}$Sr$_x$CuO$_4$ Anisimov and collaborators [510] found an effective dielectric constant of $\epsilon^*=11$ and an impurity ionization energy of $\approx 800\,\text{cm}^{-1}$.

It is important to note that the broad background, *i.e.*, the incoherent *spin* polaron contribution to $\sigma(\omega)$, does not show an appreciable temperature dependence. Whether the quasiparticles are localized by impurities (4 K) or not (300 K) does not influence the spin polaron absorption. This reveals the nature of the bound particle: it is not a bare hole, but a spin-polaron.

The simultaneous coupling of the doped carriers to both spin and lattice degrees of freedom raises a chicken-or-egg question. Electron-phonon coupling and electron-spin coupling
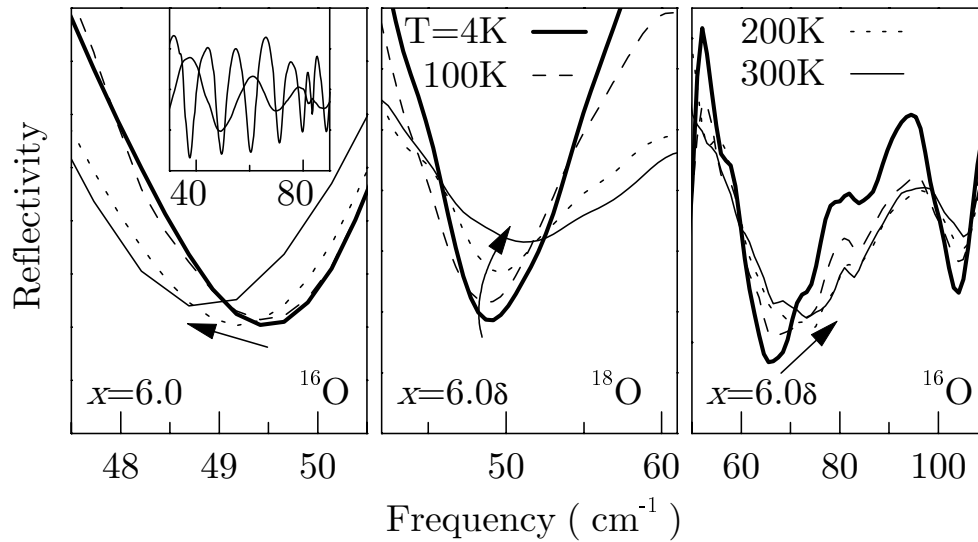
Figure 7.13: *Temperature dependent position of interference minima. The doping concentration increases from the left to the right panel. Data in the latter correspond to the highest curve in Fig. 7.8. The behavior observed in the right panel indicates a transfer of spectral weight to $\omega = 0$ with increasing temperature (see Fig. 7.14 below and main text). Inset: 4 K spectra of the samples shown in the left and mid panels on an expanded scale.*
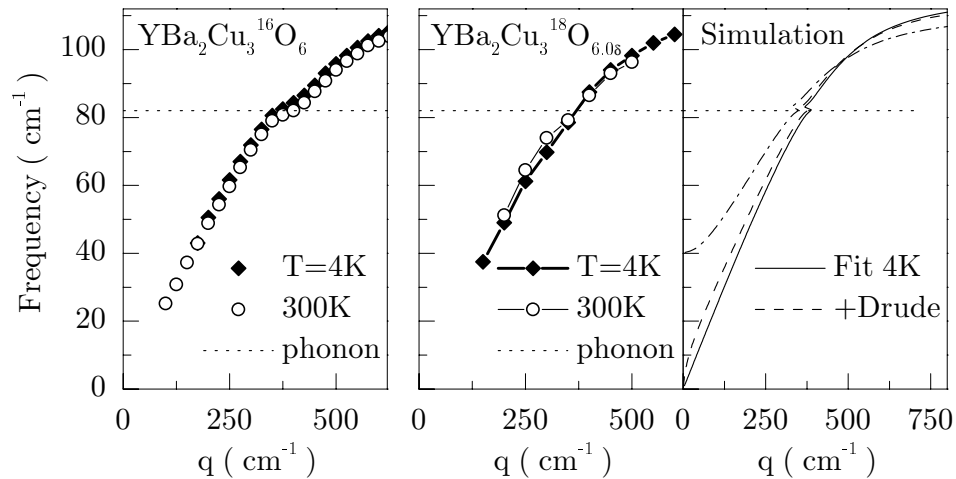
Figure 7.14: *Polariton dispersion at 4 and 300 K derived from the interference extrema of the same samples as shown in the inset and the left and mid panels of Fig. 7.13 above. The simulation in the right panel refers to the transfer of spectral weight in the low doped case. The solid line was derived from a fit of 4 K data of an undoped sample; the dashed line was obtained by (i) adding a small Drude peak with $\omega_0 = 0$, $\omega_p = 100$ cm^{-1} and $\gamma = 25$ cm^{-1}, and (ii) shifting the 115 cm^{-1} phonon by 0.9 cm^{-1} to the lower 300 K position. For the dash-dotted line we used $\omega_p = 200$ cm^{-1} and a phonon redshift of 5 cm^{-1}.*
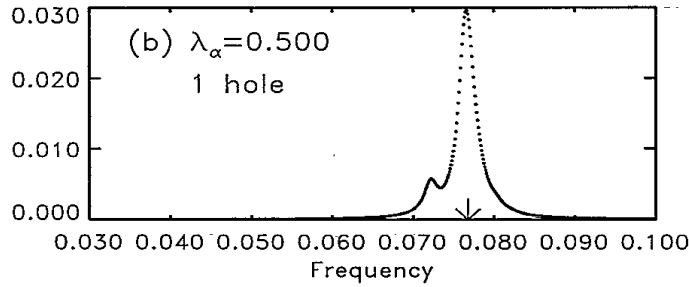
Figure 7.15: *Absorption spectrum of the planar Cu-O stretching phonon mode for the case of one doped hole as calculated by Yonemitsu, Bishop and Lorenzana [502] in the three-band Peierls-Hubbard model. A moderate electron-phonon coupling constant of $\lambda = 0.5$ is assumed, which produces a peak on the low frequency side of the phonon.*

reinforce each other [511]. The electronic correlations renormalize the bandwidth, *i.e.*, the kinetic energy of the holes is no longer large compared to the lattice polaron binding energy. Without the coupling to the spin background in the first place the electron-phonon coupling would not be strong enough in the cuprates to trap the doped holes. On the other hand, a further increase of the electron-spin coupling makes the electron-phonon interaction even more effective, as observed in the $S = 1$ nickelates [512]. If λ were large on its own, then already the *bare* hole would be trapped by the lattice and the contribution of the magnetic polaron to $\sigma(\omega)$ would be suppressed. In terms of $\sigma(\omega)$ this means that both electron-spin and electron-phonon interaction suppress the Drude contribution centered at $\omega = 0$ and shift spectral weight to finite frequencies. With increasing temperature the electron-phonon part of this spectral weight transfer is neutralized, but this hardly affects the broad background.

A further indication for a lattice contribution to the absorption process at $1050\,\mathrm{cm^{-1}}$ is given by the different behavior of the oxygen isotope substituted $YBa_2Cu_3{}^{18}O_{6+y}$ sample. There, the temperature dependence (Fig. 7.12) is similar above the peak frequency, but more complicated below, where $\sigma(\omega)$ is *higher* at 100 K than at 4K. Also the peak frequency seems to depend on the oxygen isotope, shifting from about $1050\,\mathrm{cm^{-1}}$ in $YBa_2Cu_3{}^{16}O_{6+y}$ to $1450\mathrm{cm^{-1}}$ in $YBa_2Cu_3{}^{18}O_{6+y}$. However, it is possible that the feature in $YBa_2Cu_3{}^{16}O_{6+y}$ consists of *two* peaks, one at $1050\,\mathrm{cm^{-1}}$ and one at $1450\mathrm{cm^{-1}}$, and the latter one dominates at lower doping levels (see arrows in Fig. 7.9; note also Fig. 7.11). Speculating about a possible origin for a distinct peak at $1450\ \mathrm{cm^{-1}}$ we note that an exact diagonalization study of the *t-J* model shows a peak in $\sigma(\omega)$ at $1.7J$ [242] (see thin solid line in Fig. 7.1), corresponding to $\approx 1350\,\mathrm{cm^{-1}}$ in $YBa_2Cu_3O_6$.

Based on a Hartree-Fock study Yonemitsu and co-workers [502] proposed that already for moderate values of electron-phonon coupling the relaxation of the lattice around a magnetic polaron will give rise to a local phonon mode (see Fig. 7.15). We identify this local mode with the side peak of the in-plane Cu-O bond stretching phonon mode at 500 $\mathrm{cm^{-1}}$ for $x=6.1$, 6.2 and 6.3 (see Fig. 7.16). The temperature dependence of this side peak is identical to the one of the magneto-elastic polaron peak at $1050\ \mathrm{cm^{-1}}$ (compare top panel of Fig. 7.12), which corroborates the assignment. A similar behavior was observed in $Nd_2CuO_{4-\delta}$ [424, 513] (see Fig. 4.19 on page 127 for the 4 K data).

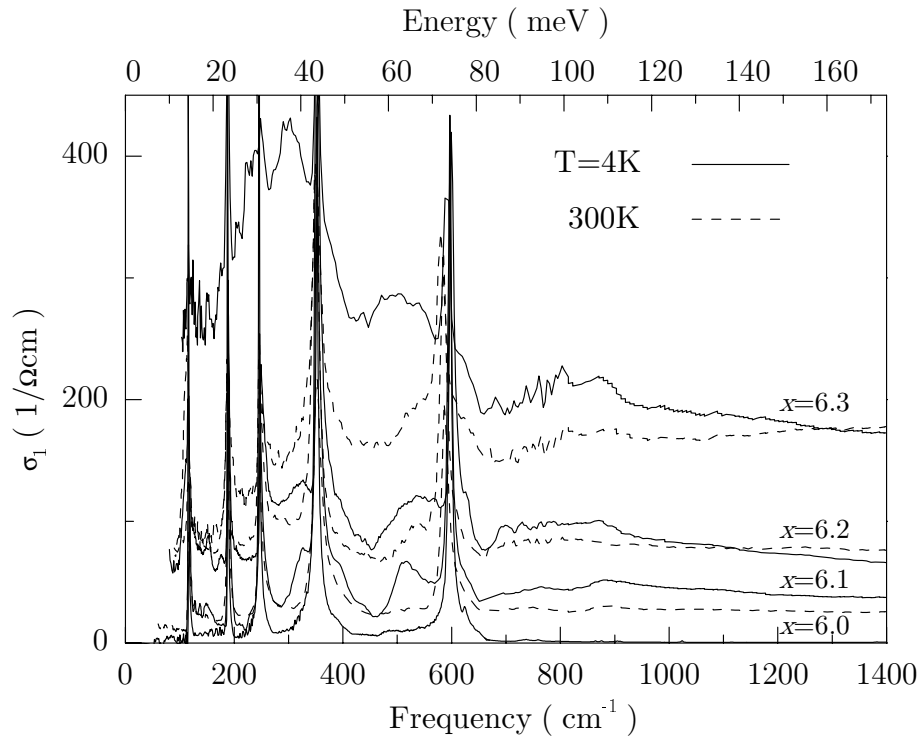All absorption processes described here can also be observed at higher doping levels (see

Figure 7.16: *Temperature dependence of $\sigma(\omega)$ of $YBa_2 Cu_3 O_x$ at intermediate doping concentrations. Data for $x \geq 6.1$ are reproduced from Münzel [501]. The broad peak at about 1000 cm^{-1}, the peak at 500 cm^{-1} (see Fig. 7.15) and the shoulder on the high frequency side of the stretching phonon mode at $600\,cm^{-1}$ (see discussion in chapter 4) are all present at all doping levels at low temperatures.*

Fig. 7.16). With increasing doping a strong increase of the broad background occurs. All samples show the photo-ionization peak of the magneto-elastic polaron and its suppression at higher temperatures. A Drude-like peak develops only for $x \geq 6.3$.

In conclusion, we have observed that very low doping of $YBa_2Cu_3O_6$ produces spectral weight at all frequencies below the charge transfer gap, as expected for an insulating correlated electron system. We have shown that the interactions of the doped carriers with both spin and lattice degrees of freedom are crucial to understand $\sigma(\omega)$ in low doped $YBa_2Cu_3O_x$.